To Appear in the Astrophysical Journal Supplements
Preprint typeset using LaTeX style emulateapj v. 21/08/00

ACCURATE REDSHIFTS AND CLASSIFICATIONS FOR 110 RADIO-LOUD AGNS

Michael Eracleous[1,2]
Department of Astronomy and Astrophysics, The Pennsylvania State University, 525 Davey Lab, University Park, PA 16803
AND

Jules P. Halpern[1]
Department of Astronomy, Columbia University, 550 West 120th St., New York, NY 10027
To Appear in the Astrophysical Journal Supplements

ABSTRACT

We report accurate redshifts of 110 active galaxies (mostly radio-loud objects at $z < 0.4$) observed in the course of a survey to find broad, double-peaked emission lines. These redshifts are measured from the narrow emission lines of these objects and are accurate to at least one part in 10^4. For each object we determine a redshift from high- and low-ionization lines separately, as well as an average redshift from all the available lines. We find that in about 15% of cases, the low-ionization lines yield a slightly higher redshift than the high-ionization lines; the average redshift difference amounts to a velocity difference of approximately 80 km s^{-1}. In addition to the redshift measurements we also report revised redshifts for two objects as well as new classifications for three narrow-line objects.

Subject headings: galaxies: active – quasars: emission lines – line: identification – galaxies: distances and redshifts

1. INTRODUCTION

In the process of searching for broad, double-peaked Balmer emission lines in moderate redshift, radio-loud active galactic nuclei (AGNs) we surveyed 108 objects taken from AGN catalogs, *circa* 1991. A detailed analysis of the results of this survey have been presented in Eracleous & Halpern (1994, 2003, hereafter papers I and II), where a description of the observations and data reduction can also be found. In this paper we report the redshifts measured from the spectra of *all* objects observed in this survey, including spectra presented in paper I. The motivation for these redshift measurements is that values accurate to $\delta z \sim 10^{-4}$ are often needed for specific applications (e.g., narrow-band imaging), while the cataloged values have a precision of $\delta z \sim 10^{-3}$. More importantly, we also find that the values that we measure sometimes disagree with the cataloged values at the level of $\delta z \sim 10^{-3}$, and on some occasions at the level of $\delta z \sim 10^{-2}$. Here we present redshifts, along with estimated uncertainties which are of the order of $\delta z \sim 10^{-4}$, and often of the order of $\delta z \sim$ a few $\times 10^{-5}$.

In the process of acquiring the data we also observed 12 objects which had only narrow emission lines and seven objects whose redshifts were higher than 0.4. The spectra and revised redshifts of the first set of such objects were presented in paper I. The second set of such objects were observed after paper I was published and their spectra are included in this paper for completeness (they were not included in paper II so as to keep that paper short and focused).

2. REDSHIFT MEASUREMENTS

Our sample of objects consists of 89 objects from paper I, 19 objects from paper II, plus Arp 102B and S4 0954+65 and includes broad-line objects, as well as small number of narrow line objects (see paper I and §2, below). The object S4 0954+65 is a blazar, which was included in our sample unintentionally; we report its redshift here for completeness. Its spectrum is shown by Lawrence et al. (1996). The spectra used for redshift determination were obtained during several observing runs between 1988 and 2000 at the Kitt Peak National Observatory's and Cerro Tololo Interamerican Observatory's 4m telescopes, the Lick Observatory's 3m telescope, the MDM Observatory's 2.4m telescope and the Kitt Peak National Observatory's 2.1m telescope. We targeted the Hα lines of objects in the redshift range $z < 0.4$ thus, most of our spectra typically span a wavelength range starting between 6,000 and 6,600 Å and ending between 9,500 and 10,000 Å, with a resolution of 6–9 Å. For objects with $z < 0.1$, we obtained several spectra of the Hα and Hβ region with starting wavelengths between 3,800 and 4,600 Å and ending wavelengths between 7,400 and 8,500 Å. In a few cases we also observed objects with $0.1 < z < 0.4$ at wavelengths as short as 3,200 Å. As a result of the above observing strategies, the lines most often available for redshift measurements were Hα and the low-ionization forbidden lines in its immediate vicinity (we were able to measure Hα in 92% of objects, [N II] λ6583 and [O I] λ6300 in 2/3 of the objects each, and at least one of the lines of the [S II] doublet in approximately half of the objects). The most commonly measured high-ionization lines were those of the [O III] $\lambda\lambda$4959,5007 doublet (available in about half of the objects, along with Hβ). Finally in about 10–20%

[1] Visiting astronomer, Kitt Peak National Observatory, which is operated by the AURA, Inc., under agreement with the National Science Foundation

[2] Visiting astronomer, Cerro Tololo Inter-American Observatory, which is operated by the AURA, Inc., under agreement with the National Science Foundation

of objects, we were able to measure lines in the blue/near-UV part of the spectrum, namely He II, [O III] λ4363, Hγ, [Ne III], [O II], and Mg II.

Redshifts were determined by measuring the observed wavelengths of reasonably strong *narrow* emission lines from all available spectra. A list of the lines that have proven useful in this respect is given in Table 1, where we also identify which lines we regard as high- and low-ionization lines. The rest wavelengths of these lines were taken from Kaler et al. (1976). In the case of the [O II], and Mg II doublets, which are always unresolved in our spectra, we adopted the average wavelength of the doublet as the rest wavelength to be compared with our measurements. The line wavelengths were measured by fitting a Gaussian to several pixels around the line peak (typically 7 to 11 pixels). Thus measurements were made using only lines with clearly discernible peaks – no attempt was made to de-blend line complexes in which the line peaks were not well separated. This technique allows us to locate the peak of the line to better than a pixel, in particular to 0.30 pixels 50% of the time and 0.48 pixels 68% of the time. After suitable heliocentric velocity corrections the wavelengths of all lines from the same object were used to determine its redshift. A redshift and associated uncertainty were determined separately from low- and high-ionization lines, and a mean redshift and associated uncertainty were also determined using all available lines. The uncertainty in the redshift was estimated as follows:

- If two or more lines from the same object were available, the uncertainty in the redshift was taken to be the adjusted error in the mean, $s_{\rm n-1}$, given by (e.g., Barford 1985)

$$s^2_{\rm n-1} \equiv \frac{\sigma^2}{n-1} = \frac{1}{n(n-1)} \sum_{i=1}^{n} (\bar{z} - z_{\rm i})^2, \quad (1)$$

  where $\bar{z}$ is the mean redshift, n is the number of lines used, and $z_{\rm i}$ is the redshift derived from an individual line (σ is the usual root-mean-squared dispersion about the mean). We note that $s_{\rm n-1}$ is related to the more usual error in the mean, $s_{\rm n}$, by $s_{\rm n-1} = s_{\rm n}\ \sqrt{n/(n-1)}$, where the factor $\sqrt{n/(n-1)}$ effectively takes into account the fact that the sample has a finite membership (see Barford 1985 for a more detailed discussion). This statistical estimate of the uncertainty accounts for several sources of error, such as errors in locating the line peaks, and errors in the relative wavelength calibration of a spectrum. If more than one spectrum is used, then errors resulting from absolute differences in the wavelength scales of individual spectra are also accounted for. However, this method does not account for possible skewness or asymmetry of the line profiles, and also assumes that all lines used in the redshift determination have the same intrinsic redshift.

- If only a single emission line from a particular object was available, the uncertainty in the redshift was estimated from the accuracy with which the line peak can be located, namely the 68% confidence limit of 0.48 pixels quoted above. This limit was determined by considering the dispersion about the mean redshift in objects where two or more emission lines were available. As a result, it is not necessarily an accurate estimate of the uncertainty in the redshift of a particular object, but it does account for possible errors in the wavelength calibration in an average sense, as well as errors in locating the line peak.

The following sources of error deserve special mention and discussion. All of these effects are captured by our statistical method for estimating error bars.

1. Systematic uncertainties associated with wavelength calibration are of the order of a few $\times 10^{-5}$.

2. The peaks of narrow lines that lie on the sloping wings of broad lines could be slightly shifted. This is an issue with the Balmer and [N II] lines in most objects and also with the [S II] doublet, which lies on the red wind of the broad Hα line in about 15% of our objects. To assess the magnitude of the effect, we carried out tests in the most extreme cases of [S II] doublets. The tests consisted of comparing the peak wavelengths measured with and without subtracting the underlying sloping pseudo-continuum. We found that the difference in the results translates into a median redshift difference of several $\times 10^{-5}$, which is comparable to the uncertainty in wavelength calibration.

3. The presence of Fe II lines in the vicinity of the [O III] $\lambda\lambda$4959,5007 doublet could affect the measurement of the peaks of these lines. This could be important because these lines are the most commonly measured high-ionization lines. We therefore inspected all of our spectra and did not find any cases with discernible Fe II lines in the regions of interest; thus we made no attempt to remove them. The absence of Fe II lines is understandable since the vast majority of our objects are double-lobed radio sources.

The measured redshifts are given in Table 2, which includes the mean redshift (from all available lines), the low-ionization line redshift and the high-ionization line redshift. Figures in parenthesis give the uncertainty in the last digit of the reported redshift. For reference the table also gives the number of spectra and the number of low- and high-ionization lines used.

3. REDSHIFT DIFFERENCES BETWEEN LOW- AND HIGH-IONIZATION LINES

To investigate whether the low- and high-ionization lines yield significantly different redshifts, we have computed the difference between these two redshifts for the 55 objects where both measurements were available. The redshift difference was normalized by the its uncertainty[3], to

[3] The uncertainty in the redshift difference was computed as $s_{\rm LH} = (s^2_{\rm LIL} + s^2_{\rm HIL})^{1/2}$, where $s_{\rm LIL}$ and $s_{\rm HIL}$ are the uncertainties in the redshifts of the low- and high-ionization lines, respectively, given in Table 2

give $(z_{\rm LIL} - z_{\rm HIL})/s_{\rm LH}$, and its distribution is shown in the histogram of Figure 1. If the scatter in the redshift differences is entirely the result of measurement errors, then we would expect the shape of the histogram to resemble a Gaussian with unit standard deviation. Therefore, we have overlaid in Figure 1 such a Gaussian, normalized so that its mean square deviation from the bins of the histogram is minimized. A visual comparison of this expected Gaussian distribution with the observed histogram shows them to agree at negative values of the redshift difference. At positive values, however, there appears to be an excess of objects with $(z_{\rm LIL} - z_{\rm HIL})/s_{\rm LH} > 2$, which suggests that in some cases the low-ionization lines yield a larger redshift than the high-ionization lines. Isolating and examining the objects that make up this excess, we find a mean velocity difference between low- and high-ionization lines of $c\langle z_{\rm LIL} - z_{\rm HIL}\rangle \approx 80$ km s^{-1}. Although this result is interesting, it needs to be verified using a much larger sample of objects. If we accept it at face value, it may indicate a stratification of the narrow-line region. More specifically, in the context of a scenario in which the narrow-line region gas is outflowing, this result implies that the high-ionization lines arise in gas that is further away from the center and possibly of lower density.

Redshift differences between high- and low-ionization lines in Seyfert galaxies and narrow-line radio galaxies have been known for quite some time. Koski (1978) compiled a list of 6 cases with redshift differences of a few hundred km s^{-1} (600 km s^{-1} in the extreme case of I Zw 1), while Whittle (1985) and Veilleux (1991) found differences of $\lesssim 100$ km s^{-1} between the centroid of the [O III] λ5007 line and the systemic velocity of the host galaxy. A more recent study of a wide variety of AGNs by Marziani et al. (2003) yielded similar redshift differences between the [O III] λ5007 and Hβ lines and also identified outliers with large redshift differences of order several hundred km s^{-1}. In the vast majority of cases the high-ionization lines are blueshifted relative to the low-ionization lines, a trend which supports the hypothesis that the narrow-line gas is outflowing from the nucleus. The results of individual case studies of nearby narrow-line AGNs that map the kinematics of the gas support this hypothesis as well (e.g., Cygnus A by Taylor, Tadhunter, & Robinson 2003 and NGC 1068 by Cecil, Bland, & Tully 1990).

4. NARROW-LINE OBJECTS AND NEW REDSHIFTS

Three objects listed in paper II, PKS 0511–48, 3C 381, and 3C 456, were found to have only narrow emission lines; their spectra are shown in Figure 2. The radio galaxy 3C 381 was included in our survey because of a report of a broad Hα line by Grandi & Osterbrock (1978). These authors noted that the signal-to-noise ratio (S/N) of the 3C 381 spectrum was low, but the spectrum was not shown and the exact date of observation was not given (from indirect remarks we infer that the observations were probably obtained in the early 1970s). A spectrum of 3C 381 obtained in 1982 by Saunders et al. (1989) covering the rest-frame range 3100–6100 Å with moderate S/N shows no broad lines. Our own spectrum shows this object as a narrow-line radio galaxy. In view of the available data we conclude that 3C 381 has either lost its broad lines some time in the past 20 years, or Grandi & Osterbrock (1978) were misled in their detection of a broad Hα line by the low S/N of their spectrum.

Three objects listed in paper II, 4C 72.16, PKS 1355–12 and PKS 2312–319, were found to have grossly incorrect cataloged redshifts; as a consequence, their Hα lines did not fall within the observed spectral range. These objects were included in our target list because their redshifts listed in Véron-Cetty & Véron (1989) were lower than 0.4. Since then 4C 72.16 was observed by Jackson & Browne (1991) who reported a redshift of 1.46, in agreement with our own measurement; a plot of the spectrum can be found in that paper. An incorrect redshift for 4C 72.16 of 0.357 was originally reported by Arp, de Ruiter, & Willis (1979), who noted that it was insecure. PKS 1335–12 was observed by Stickel, Kuhr, & Fried (1993) who measured a redshift 0.539, in agreement with the value that we obtain. The spectrum of this object presented in Figure 3 covers a different spectral range than that of Stickel et al. (1993). The redshift of PKS 2312–319 was reported to be 0.284 by Jauncey et al. (1982), based on the identification of a single line at 3592 Å as Mg II λ2800 (this line was observed in an unpublished spectrum by R. G. Clowes, R. D. Cannon, and A. Savage taken in 1980). We obtain a redshift of 1.322 based on the identification of several emission lines. In view of this redshift, the single emission line observed by Clowes et al. must have been C IV λ1550, which is also the strongest line in our own spectrum. The spectrum of this object is shown in Figure 3 where we also identify the lines that we used to determine its redshift.

We thank the anonymous referee for thoughtful comments and suggestions. We acknowledge partial support from NASA through grant GO-08684.01-A from the Space Telescope Science Institute, which is operated by the Association of Universities for Reasearch in Astronomy, Incorporated, under NASA contract NAS5-26555.

REFERENCES

Arp, H. C., de Ruiter, & Willis 1979, A&A, 77, 86
Barford, N. C. 1985, Experimental Measurements: Precision, Error and Truth, 2nd ed. (Chichester: Wiley), 26
Cecil, G., Bland, J., & Tully, R. B. 1990, ApJ, 355, 70
Eracleous, M., & Halpern, J. P. 1994, ApJS, 90, 1 (paper I)
Eracleous, M., & Halpern, J. P. 2003, ApJ, 599, in press (astro-ph/0309149; paper II)
Grandi, S. A., & Osterbrock, D. E. 1978, ApJ, 220, 783
Halpern, J. P., & Eracleous, M. 2000, ApJ, 531, 647
Jackson, N., & Browne, I. W. A. 1991, MNRAS, 250, 422
Jauncey, D. L., Batty, M. J., Gulkis, S. & Savage, A. 1982, AJ, 87, 763
Kaler, J. B., Aller, L. H., Czyzak, S. J., & Epps, H. W. 1976, ApJS, 31, 163
Koski, A. 1978, ApJ, 223, 56
Lawrence, C. R., Zucker, J. R., Readhead, A. C. S., Unwin, S. C., Pearson, T. J., & Xu, W. 1996, ApJS, 107, 541
Marziani, P., Zamanov, R., Sulentic, J. W., Calvani, M., & Dultzin-Hacyan, D. 2003, Mem. S. A. It., 74, 492
Saunders, R., Baldwin, J. E., Rawlings, S., Warner, P. J., & Miller, L. 1989, MRAS, 238, 777
Stickel, M., Kuhr, H., & Fried, J. W. 1993, A&AS, 97, 483
Taylor, M. D., Tadhunter, C. N., & Robinson, T. G. 2003, MNRAS, 342, 995
Veilleux, S. 1991, ApJS, 75, 383
Véron-Cetty M. P., Véron P. 1989, "A Catalogue of Quasars and Active Galactic Nuclei (4th Edition)" ESO Scientific Report No. 7 (Garching bei Munchen: ESO)
Whittle, M. 1985, MNRAS, 213, 1

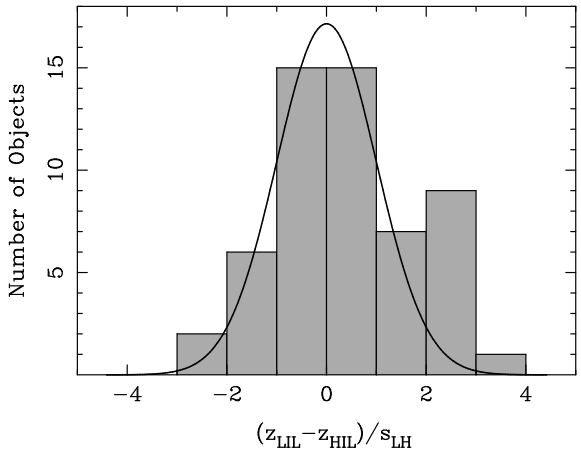

FIG. 1.— The distribution of redshift differences between low- and high-ionization lines normalized by its uncertainty. The histogram includes 56 objects for which the necessary measurements were available. The thick solid line is a Gaussian of unit standard deviation, normalized so as to minimize its mean square deviation from the bins of the histogram.

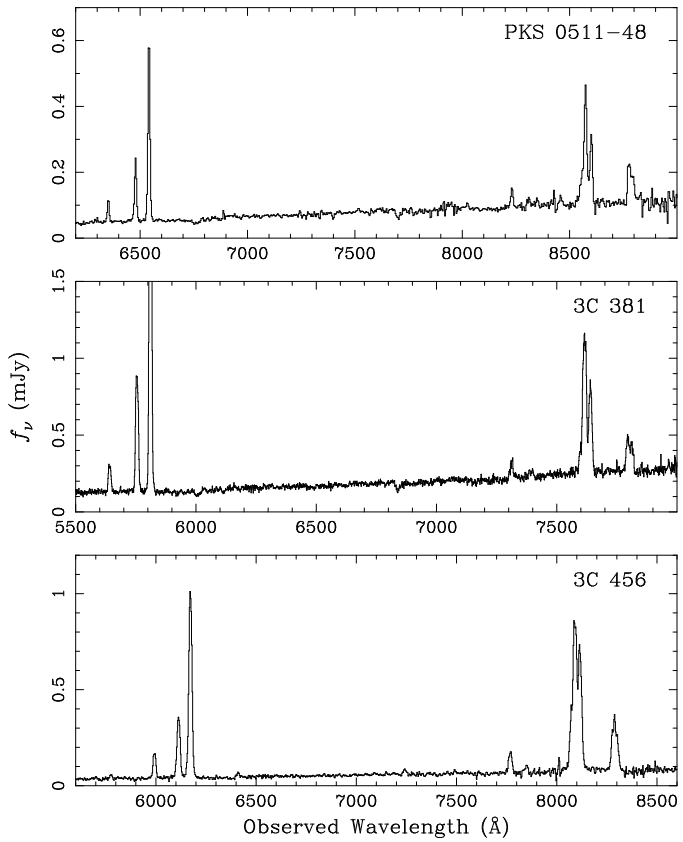

FIG. 2.— Spectra of three objects found to have only narrow emission lines. These were reported as broad-line objects in the literature.

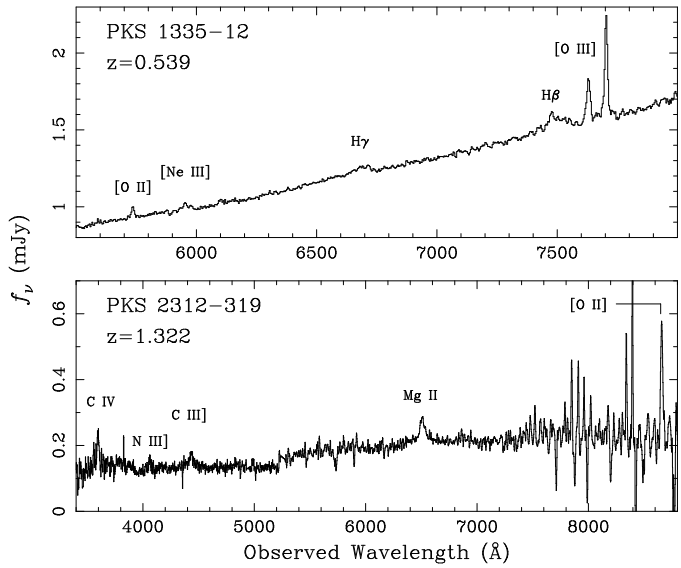

FIG. 3.— Spectra of two objects with incorrect redshifts reported in the literature. The line identifications on which our redshift determinations are based are marked, and the measured redshifts are given in the figure.

Table 1
Emission Lines Used for Redshift Determinations and Adopted Rest Wavelengths

Ion and Transition	Adopted Wavelength (Å)	Low/High Ionization
Mg II λ2796,2803	2799.12	L
[O II] $\lambda\lambda$3726,3729	3727.37	L
[Ne III] λ3869	3868.75	H
Hγ	4340.53	L
[O III] λ4363	4363.21	H
He II λ4686	4685.75	H
Hβ	4861.30	L
[O III] λ4959	4958.95	H
[O III] λ5007	5006.88	H
[O I] λ6300	6300.31	L
[O I] λ6363	6363.82	L
[N II] λ6548	6548.09	L
Hα	6562.96	L
[N II] λ6583	6583.36	L
[S II] λ6717	6716.52	L
[S II] λ6331	6730.74	L

Table 2
Measured Redshifts[a]

Object	$\bar{z}$	$z_{\rm LIL}$	$z_{\rm HIL}$	Spectra	LILs	HILs	Notes[b]
4C 25.01	0.2844(2)	0.2844(2)	...	1	3		
3C 17	0.22024(7)	0.22019(7)	0.2205(1)	2	15	3	
MRC 0041+119	0.2261(3)	0.2263(3)	0.2258(5)	1	3	3	
PKS 0105–00[c]	1.375(1)	1.375(1)	...	1	1		new z
B2 0110+29	0.3627(2)	0.3627(2)	...	1	3		
PKS 0152–51[c]	1.582(1)	1.582(1)	...	1	1		new z
4C 31.06	0.37334(8)	0.37342(9)	0.3732(1)	1	5	3	
PKS 0202–76	0.38925(4)	0.38930(2)	0.38919(6)	1	3	2	
3C 59	0.1096(1)	0.1096(1)	...	2	10		
PKS 0214+10	0.4070(1)	0.4070(2)	0.40709(2)	1	2	2	
3C 67	0.3107(2)	0.3107(2)	...	1	3		
PKS 0235+023	0.2072(1)	0.2072(1)	...	2	9		
IRAS 0236.6–3101	0.06233(3)	0.06233(3)	...	1	5		
4C 39.11	0.16099(3)	0.16099(3)	...	1	5		
PKS 0312–77	0.2250(5)	0.2250(5)	...	1	3		
PKS 0340–37	0.28513(4)	0.28509(5)	0.28526(3)	3	15	5	
3C 93	0.35730(6)	0.35728(9)	0.35735(1)	2	6	2	
3C 93.1	0.24425(9)	0.24425(9)	...	1	5		NLRG
3C 111	0.04907(6)	0.04909(9)	0.04902(2)	1	5	2	
3C 119	1.0221(3)	1.0221(7)	1.02207(1)	1	2	1	new z
MS 0450.3–1817	0.06161(7)	0.06161(7)	...	2	11		
PKS 0511–48	0.30638(4)	0.30636(6)	0.30641(2)	1	4	2	NLRG
3C 135	0.1273(1)	0.1273(1)	...	1	6		NLRG
Pictor A	0.03498(5)	0.03495(5)	0.0350(1)	1	6	3	
PKS 0558–50	0.1379(2)	0.1379(2)	...	1	1		
3C 171	0.2382(1)	0.2382(1)	...	1	5		NLRG
PKS 0723–008	0.1273(1)	0.1273(1)	...	1	6		NLRG
B2 0742+31	0.46134(1)	0.46134(2)	0.46134(2)	3	4	6	
PKS 0812+02	0.4028(2)	0.4028(2)	...	1	2		
CBS 74	0.09190(2)	0.09188(2)	0.091974(6)	2	17	5	
3C 206	0.1973(1)	0.1973(1)	...	1	5		
DW 0839+187	1.2724(4)	1.2724(4)	...	1	1		new z
PKS 0846+10	0.36546(9)	0.36546(9)	...	1	2		
PKS 0857–19	0.3608(1)	0.3608(1)	0.36081(8)	1	5	2	
4C 5.38	0.30157(3)	0.30160(3)	0.30151(2)	1	5	2	
PKS 0921–213	0.05308(2)	0.05306(2)	0.05313(5)	2	12	6	
PKS 0925–203[d]	0.34735(9)	0.3475(1)	0.34723(2)	1	2	2	
3C 227	0.08603(5)	0.08608(6)	0.0859(1)	4	14	7	
4C 9.35	0.29809(2)	0.29809(3)	0.29808(2)	1	5	2	
S4 0954+65	0.3675(2)	0.3675(2)	...	1	3		blazar
PKS 1004–21[d]	0.33046(7)	0.33053(1)	0.3303(4)	1	2	1	
PKS 1004+13	0.2406(1)	0.2406(1)	...	1	4		
PKS 1011–282	0.2549(1)	0.2549(1)	...	1	4		
PKS 1020–103	0.1965(1)	0.1965(1)	...	3	10		
B2 1028+31	0.17785(9)	0.17785(9)	...	1	5		
3C 246	0.34545(7)	0.3455(2)	0.345421(2)	1	2	2	
PG 1049–006	0.3585(6)	0.3585(6)	...	1	5		
4C 72.16[c]	1.462(1)	1.462(1)	...	1	1		new z
PKS 1101–32	0.35547(5)	0.35553(7)	0.35538(2)	1	3	2	
4C 36.18	0.39220(3)	0.39219(5)	0.39224(2)	2	10	5	
B2 1128+31	0.2897(1)	0.2899(2)	0.28954(2)	1	1	2	
PKS 1146–037	0.34056(8)	0.34056(8)	...	1	6		
LB 2136	0.33345(4)	0.33345(4)	...	1	4		

TABLE 2—*Continued*

Object	$\bar{z}$	$z_{\rm LIL}$	$z_{\rm HIL}$	Spectra	LILs	HILs	Notes[b]
PKS 1151–34	0.25799(6)	0.25801(7)	0.2579(1)	4	23	7	
TEX 1156+21	0.3472(2)	0.3472(2)	...	1	1		
B2 1208+32A	0.38879(9)	0.38879(9)	...	1	2		
PKS 1215+013	0.11715(1)	0.11715(1)	...	1	5		NLRG
B2 1223+25	0.2679(1)	0.2678(2)	0.2680(3)	1	3	1	
PKS 1232–24	0.35512(6)	0.35507(9)	0.35522(1)	1	4	2	
3C 277.1	0.3198(2)	0.3198(2)	...	1	5		
PKS 1254–33	0.19048(9)	0.19048(9)	...	1	2		
B2 1255+37	0.7092(2)	0.7090(3)	0.7093(3)	1	1	2	new z
PKS 1302–102	0.27825(8)	0.27825(8)	...	1	2		
PKS 1304–215	0.12666(9)	0.12666(9)	...	1	5		NLRG
3C 287.1	0.21574(5)	0.21574(5)	...	1	6		
PKS 1335–12	0.5386(1)	0.5384(4)	0.53869(7)	1	1	2	new z
PKS 1346–11	0.3407(1)	0.3408(1)	0.34050(4)	1	4	2	
B2 1351+26	0.30763(7)	0.30763(7)	...	1	3		
PKS 1355–41	0.3145(1)	0.3145(2)	0.314657(6)	1	3	2	
Mkn 668	0.07681(7)	0.07688(8)	0.07665(6)	4	9	4	
PKS 1417–19	0.12039(9)	0.12039(9)	...	1	5		
PKS 1421–38	0.4068(2)	0.4068(3)	0.40687(1)	1	3	2	
CSO 643	0.27615(3)	0.27615(3)	0.27616(3)	2	10	4	
3C 303	0.14121(5)	0.14121(5)	...	1	7		
PKS 1451–37	0.3143(2)	0.3143(3)	0.31428(2)	1	6	2	
4C 37.43	0.37086(7)	0.3708(1)	0.37092(6)	1	3	3	
PKS 1514+00	0.0526(2)	0.0528(2)	0.0521(2)	1	6	2	
LB 9743	0.2536(1)	0.2536(1)	...	1	4		
4C 35.37	0.1565(2)	0.1565(2)	...	1	5		
4C 18.47	0.34647(7)	0.34647(7)	...	1	3		
3C 332	0.15098(2)	0.15099(2)	0.150910(9)	3	16	2	
MRC 1635+119	0.1474(2)	0.1474(2)	...	1	3		
3C 351	0.37194(4)	0.37189(6)	0.37200(4)	2	4	3	
Arp 102B	0.02436(3)	0.02437(3)	0.02436(6)	3	27	12	
B2 1719+35	0.28345(3)	0.28344(4)	0.28348(2)	1	6	2	
B2 1721+34	0.2053(1)	0.2053(1)	...	1	4		
PKS 1725+044	0.29662(8)	0.29662(8)	...	1	4		
PKS 1739+18C	0.18588(6)	0.18595(8)	0.18577(2)	1	3	2	
MRC 1745+16	0.3919(1)	0.3919(1)	0.39185(2)	1	6	2	
3C 381	0.16058(4)	0.16061(6)	0.16052(5)	2	10	7	NLRG
3C 382	0.05807(5)	0.05806(6)	0.058156(8)	4	17	2	
3C 390.3	0.05550(2)	0.05551(2)	0.05548(3)	6	29	3	
PKS 1914–45	0.36378(3)	0.36376(5)	0.36381(1)	1	4	2	
PKS 2058–42	0.2232(1)	0.2232(1)	...	1	4		
PKS 2139–04	0.34390(9)	0.3440(1)	0.343780(5)	1	3	2	
OX 169[e]	0.21087(5)	0.21114(3)	0.21061(6)	12	19	20	
PKS 2159–335	0.1537(3)	0.1537(3)	...	1	2		NLRG
PKS 2208–13[d]	0.39110(8)	0.3912(2)	0.39104(1)	1	2	2	
3C 445	0.05623(2)	0.05623(2)	0.05622(5)	3	13	4	
PKS 2227–399	0.31788(7)	0.3179(1)	0.317971(8)	1	6	2	
PKS 2242–29	0.1658(2)	0.1658(2)	...	1	2		NLRG
PKS 2247+14	0.23478(8)	0.2349(1)	0.23466(5)	1	5	3	
PKS 2300–18	0.12883(6)	0.12883(6)	...	1	6		
PKS 2302–71	0.38425(6)	0.3842(1)	0.38429(2)	1	2	2	
PKS 2305+18	0.31301(4)	0.31305(4)	0.31297(7)	1	7	5	
3C 456	0.2326(2)	0.2328(2)	0.2323(4)	1	6	4	NLRG

TABLE 2—*Continued*

Object	$\bar{z}$	$z_{\rm LIL}$	$z_{\rm HIL}$	Spectra	LILs	HILs	Notes[b]
PKS 2312–319[f]	1.322(1)	1.324(2)	1.321(1)	1	2	3	new z
3C 459	0.2201(2)	0.2201(2)	...	1	4		NLRG
MRC 2328+167[d]	0.2801(5)	0.2795(3)	0.2806(9)	1	3	3	
PKS 2349–01	0.1741(1)	0.1741(1)	...	1	4		

[a] $\bar{z}$, $z_{\rm LIL}$, and $z_{\rm HIL}$ denote respectively the redshifts derived from all available lines, low-ionization lines only, and high-ionization lines only. The figure in parenthesis is the uncertainty in the last digit of the reported redshift.

[b] "NLRG" = narrow-line object, "new z" = revised redshift (from paper I or paper II).

[c] The redshift is based on the measured wavelength of the Mg II doublet only, whose peak is often broad and asymmetric, and also affected by associated absorption lines. Therefore the uncertainty is larger than usual.

[d] The only available low-ionization lines are the Balmer lines whose peaks are rather broad. This suggests that the narrow Balmer lines are extremely weak and hence the measured LIL redshift refers to the broad lines.

[e]The redshift of OX 169 was measured using all the spectra from Halpern & Eracleous (2000)

[f] The lines used for the determining the redshift of PKS 2312–319 are: C IV λ1549, N III] λ1750, C III] λ1909, Mg II λ2798, and [O II] λ3727. The signal-to-noise ratio is low and therefore the uncertainty in the redshift is larger than usual.